Article type: Communication

Title: A Thermal Radiation Modulation Platform by Emissivity Engineering with Graded Metal-Insulator Transition

Kechao Tang, Xi Wang[†], Kaichen Dong, Ying Li, Jiachen Li, Bo Sun, Xiang Zhang, Chris Dames, Chengwei Qiu, Jie Yao and Junqiao Wu[*]

K. Tang, X. Wang, K. Dong, J. Li, Prof. J. Yao, Prof. J. Wu
Department of Materials Science and Engineering, University of California, Berkeley, CA, 94720, USA
Email: wuj@berkeley.edu

K. Tang, Prof. X. Zhang, Prof. J. Yao, Prof. J. Wu
Division of Materials Sciences, Lawrence Berkeley National Laboratory, Berkeley, CA 94720, USA

Y. Li, Prof. C. Qiu
Department of Electrical and Computer Engineering, National University of Singapore, Singapore, 117583

Prof. B. Sun
Tsinghua-Berkeley Shenzhen Institute, Tsinghua University, Shenzhen 518055, China

Prof. X. Zhang
NSF Nanoscale Science and Engineering Center (NSEC), University of California, Berkeley, CA 94720, USA
University of Hong Kong, Hong Kong, China

Prof. C. Dames
Department of Mechanical Engineering, University of California, Berkeley, CA, 94720, USA

[†]Current address: Department of Materials Science and Engineering, University of Delaware, Newark, DE 19716, USA

Keywords: thermal radiation, materials platform, emissivity engineering, metal-insulator transition, infrared camouflage

Abstract

Thermal radiation from a black body increases with the fourth power of absolute temperature (T^4), an effect known as the Stefan-Boltzmann law. Typical materials radiate heat at a portion of this limit, where the portion, called integrated emissivity (ε_{int}), is insensitive to temperature ($|d\varepsilon_{int}/dT| \sim 10^{-4}/^oC$). The resultant radiance bound by the T^4 law limits our ability to regulate radiative heat. Here we show an unusual material platform in which ε_{int} can be engineered to decrease in an arbitrary manner near room temperature ($|d\varepsilon_{int}/dT| \sim 8\times10^{-3}/^oC$), enabling unprecedent manipulation of infrared radiation. As an example, we program ε_{int} to vary with temperature as inverse of T^4, precisely counteracting the T^4 dependence, hence thermal radiance from the surface becomes temperature-independent, allowing the fabrication of a flexible and power-free infrared camouflage with unique advantage in performance stability. The structure is based on thin films of tungsten doped vanadium dioxide where the tungsten fraction is judiciously graded across a thickness less than the skin depth of electromagnetic screening.

Main text paragraphs

As a strongly correlated electron material, vanadium dioxide (VO_2) features a well-known, temperature-driven metal-insulator phase transition (MIT) at $T_{MIT} = 67^oC$ [1-3]. It takes the insulating (I) phase at $T < T_{MIT}$ and abruptly switches to the metallic (M) phase at $T > T_{MIT}$. In the thermal IR spectral range near room temperature (wavelength between approximately 5 and 20 μm), the M phase of VO_2 is much more reflective than the I phase, because its plasma energy of free electrons is ~ 1 eV [4, 5], significantly higher than that of the thermal IR photons (~ 0.1eV). Therefore, much less IR energy is absorbed when VO_2 undergoes the phase transition and becomes metallic[6-9]. According to the Kirchhoff's law of radiation[10] , the spectral emissivity (λ) is equal to absorptivity in the IR regime. When averaged for thermal

radiation, an abrupt drop[11] in the integrated emissivity (ε_{int}) and hence thermal radiance is thus expected for VO_2 at $T = T_{MIT}$, as schematically illustrated in Figure1a, and experimentally measured and shown in Figure S1. Here the thermal radiance per unit solid angle is given by[12]

$$P_{rad}(T)=\int_0^\infty B(T,\lambda)(\lambda)\,d\lambda,$$

where $B(T,\lambda)=\frac{2hc^2}{\lambda^5}\frac{1}{e^{hc/(\lambda k_B T)}-1}$ is the spectral radiance of a black body, k_B is the Boltzmann constant, h is the Planck constant, c is the speed of light, λ is the wavelength, and (λ) is the spectral emissivity. Conveniently, T_{MIT} of VO_2 can be rapidly shifted from 67°C to lower temperatures, down to temperatures beyond -100°C, by doping with tungsten (W) to form $W_xV_{1-x}O_2$ alloys[13-15]. The reduction of T_{MIT} follows a rate of $dT_{MIT}(x)/dx \approx$ -25 °C/at.% as measured in our films and shown in Figure S2. The contrasts in both electrical resistivity and ε_{int} between the I and M phases are largely retained for low-fraction W doping. However, the abrupt nature of MIT in $W_xV_{1-x}O_2$ at those T_{MIT} values limits any application of the MIT to be within a narrow temperature window around T_{MIT}. This window is typically narrower than ~ 20°C (Figure S2), and outside this window, the material would behave as either a regular insulator (in the I phase) or a regular metal (in the M phase).

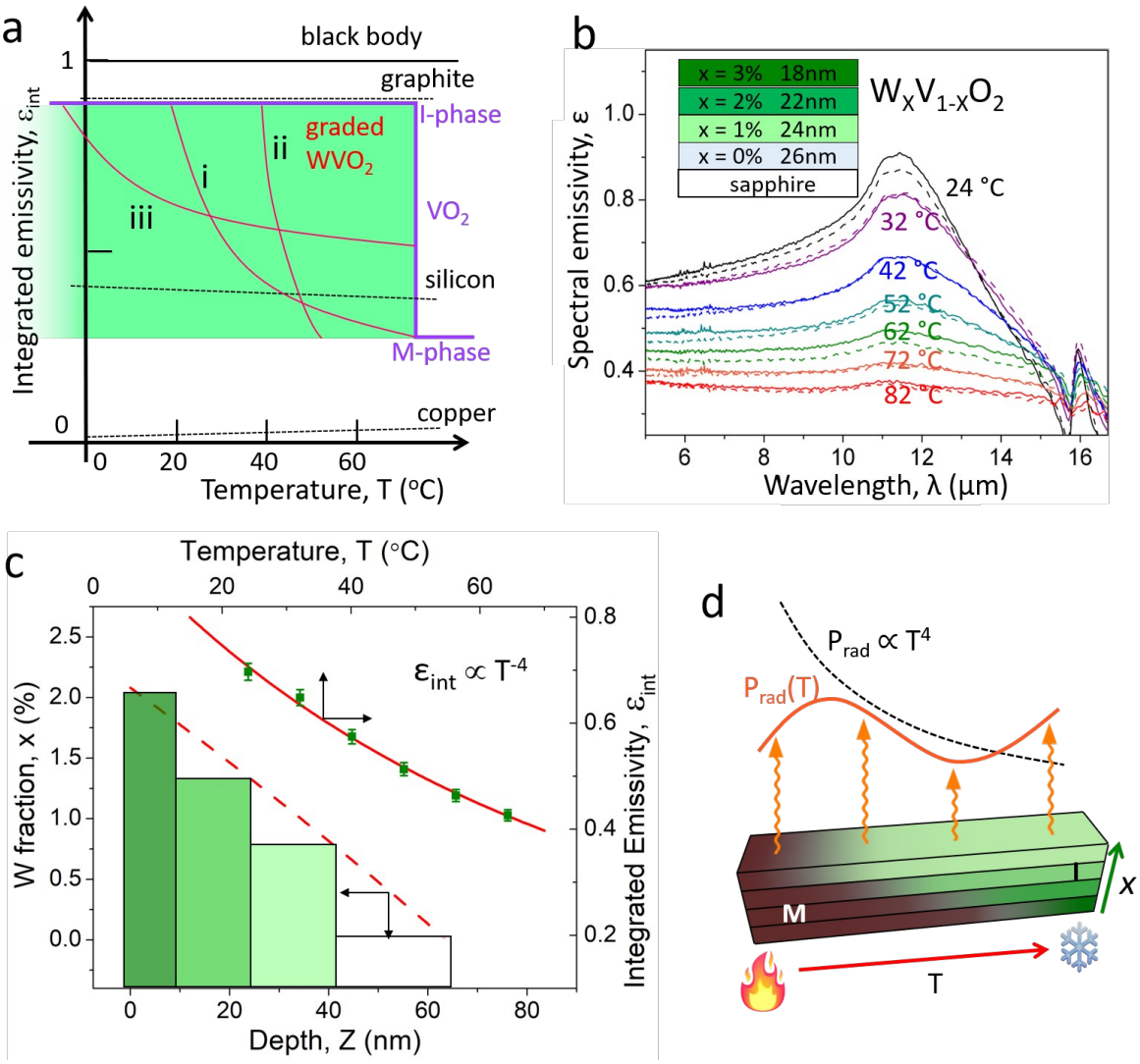

Figure 1. Engineering thermal IR emissivity by grading metal (M) - insulator (I) transition.

a. *Schematic illustrating realization of nearly arbitrary temperature dependence of integrated emissivity (ε_{int}) within the shaded area using graded W-doped VO_2, represented by the three arbitrarily designed emissivity curves denoted with i, ii and iii. The behavior of typical high, moderate and low-ε_{int} materials and of VO_2 are also shown for comparison.* ***b***. *Spectral emissivity of a graded $W_xV_{1-x}O_2$ structure (schematic in Inset) measured over a broad range of temperature, showing a smoothly but rapidly reduced ε_{int}. Solid and dashed curves correspond to data collected during heating and cooling, respectively. The spectral behavior in the long-wavelength region is related to the substrate (Figure S1&S11)* ***c***. *Design of W doping profile x(Z) (dashed line, left-bottom axes) to generate the desired $\varepsilon_{int}(T)$ relation*

(solid line, right-up axes). The boxes represent actual nominal doping profile used in the WVO_2 film deposition, and the data points are the experimentally measured $\varepsilon_{int}(T)$ from this film, which agrees well with the desired $\varepsilon_{int}(T)$. ***d****. Schematic showing that by rational design of the W doping profile (x along thickness direction) of $W_xV_{1-x}O_2$, emissivity can be programmed to regulate thermal radiation (P_{rad}) for distinctly different behavior from the Stefan-Boltzmann T^4 law.*

To overcome this limit, we designed and deposited multilayer $W_xV_{1-x}O_2$ films with total thickness less than ~ 100nm, as schematically shown in the Inset of Figure 1b. Interlayer diffusion of W took place during the film deposition and post-deposition annealing. As a result, the multilayer structure becomes a graded W-doped VO_2 film, where x varies continuously across the thickness direction (Figure S2 & S3). Indeed, the lack of kinks and abrupt changes in the electrical sheet resistance of the multilayer indicates that it becomes a smoothly graded W-doped structure. The graded doping spreads out the MIT from the original narrow temperature window near T_{MIT} to a broad temperature range spanning from $T_{MIT}(x_{max})$ to $T_{MIT}(x_{min})$. The drop in emissivity between the I and M phases becomes no longer abrupt and is also extended to this temperature range. We note that it is critical to grade the MIT within a thickness less than the skin depth (~ 130 nm) of electromagnetic screening in the M-phase, so that the emissivity for surface radiation can be modulated by the MIT progressing away from the film surface (details in Supplementary Information). The temperature dependence of (λ) of a representative graded WVO_2 film was measured using Fourier Transform IR spectroscopy (FTIR) and is shown in Figure 1b. The spectral emissivity is integrated with $B(T, \lambda)$ over the atmospheric transparency window (8 μm - 14 μm) and divided by the black body integration between the same wavelength limits to obtain $\varepsilon_{int}(T)$.

The large reduction in ε_{int} from ~ 0.75 to ~ 0.35 over a temperature range of ~ 50°C (schematic curve i in the shaded area in Figure1a), at a rate of $d\varepsilon_{int}/dT$ ~ - 8×10^{-3}/°C, is orders of magnitude stronger than that of conventional materials. For example, as schematically shown in Figure 1a, $d\varepsilon_{int}/dT$ near room temperature is about 2×10^{-5}/°C for graphite (a high-ε_{int} material)[16], -1×10^{-4}/°C for silicon (a moderate-ε_{int} material)[17], and 1×10^{-4}/°C for typical metals (low-ε_{int} materials)[18]. This temperature insensitivity of ε_{int} in conventional materials arises fundamentally from the fact that temperature variation is a small perturbation in energy with respect to typical radiative electronic and phononic processes in solids[19]. The W doping profile can be designed to be more tightly distributed across the structure to achieve even greater $|d\varepsilon_{int}/dT|$ (curve ii in Figure 1a), but at the cost of a narrower working temperature range. An example of designing the W doping profile to successfully create the desired $\varepsilon_{int}(T)$ is shown in Figure 1c (details in Supplementary Information). Therefore, this structure provides a platform where emissivity can be engineered to exhibit nearly arbitrary, strong temperature dependence beyond that of conventional materials. Following the Stefan-Boltzmann law, the thermal radiance from the surface would be regulated to have temperature dependences distinctly different from the conventional T^4 law, as depicted in Figure 1d. Exploiting the ε_{int}-regulated thermal radiation, we demonstrate a mechanically flexible and power-free thermal IR camouflage as well as a thermal IR decoy, both inherently robust and immune to drastic temporal fluctuation and spatial variation of temperature.

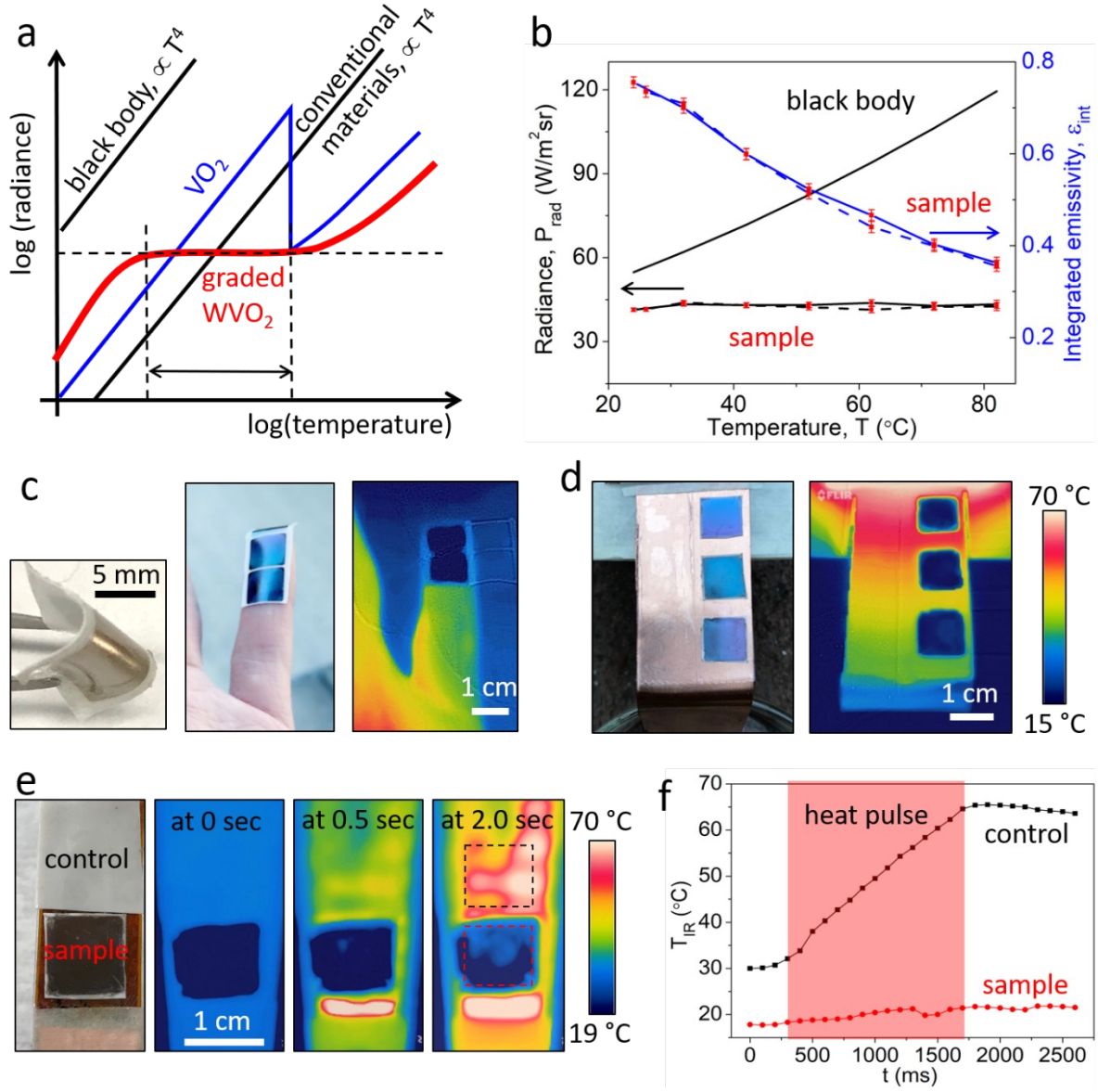

Figure 2. Mechanically flexible, power-free, and ∇T- and dT/dt-immune camouflage based on the graded WVO_2. ***a*** *Schematic illustrating constant thermal radiance over a wide range of temperature from the camouflage, in stark contrast to the Stefan-Boltzmann T^4 law from conventional materials.* ***b****. Thermal radiance and integrated emissivity of the film as a function of temperature, showing that the negative temperature coefficient of emissivity counteracts the T^4 law to yield a temperature-independent thermal radiation power. Solid and dashed curves are for measurements during heating and cooling, respectively.* ***c.*** *Optical image of a graded WVO_2 film transferred onto a PE tape showing high mechanical flexibility.*

Visible color of the sample is related to the WVO_2 thickness and lighting on surface (see experimental section). The fingertip is hidden from IR camera when covered with the camouflage. ***d****. Camouflaging an object with large spatial temperature variation from ~25°C to 65°C, showing immunity to ∇T.* ***e****. Camouflaging an object with drastic temperature surge, showing immunity to dT/dt. As shown in* ***f****, the actual temperature of the camouflage (represented by the IR temperature of the control which is a high-emissivity tape placed near the sample) rises rapidly by the heating pulse, while the IR temperature of the camouflage stays nearly flat. The IR temperature was measured by averaging the camera reading in the center 1×1 cm^2 region of each film (dashed boxes), and the error bars are comparable to the symbols in size.*

As the first example, we demonstrate a thermal IR camouflage using the graded WVO_2 platform, of which the working principle is shown in Figure 2a. When x and thickness of each layer were judiciously selected (Figure 1c), the graded doped WVO_2 exhibits an ε_{int} that depends on temperature following ~$1/T^4$. The FTIR-measured $\varepsilon_{int}(T)$ of a sample prepared following this design method (details in Figure S4) is shown in Figure 2b. The $1/T^4$ dependence of $\varepsilon_{int}(T)$ is multiplied with the Stefan-Boltzmann T^4 relation of a black body, to give the T-independent thermal radiance P_{rad}, as shown in Figure 2b. The constant P_{rad} over a temperature range over 50°C near room temperature invalidates the assumption of T-dependent P_{rad}, the principle behind IR imaging[20, 21]. As such, the structure would appear to have a constant IR temperature (T_{IR}) when imaged by an IR camera, despite the reality that its actual temperature (T_{actual}) may vary widely. Unlike low-emissivity camouflage coatings that rely on reflection signals from a confinement and thus limited to indoor scenarios, the IR

camouflage based on graded WVO_2 fools the camera by manipulating thermal radiation from the target itself, making it ideal for outdoor applications.

Existing IR camouflage techniques use a coating whose emissivity can be modulated by effects of thermochromics[22-24], electrochromics[25-28], photocarrier doping[29], or mechanical actuation[30]. These active camouflage techniques generally require energy input to operate, and are based on rigid and complicated heterostructures. They are also typically limited to only camouflage objects with uniform and slow-varying temperature profiles. In contrast, our graded-WVO_2 offers an IR camouflage that is power-free, monolithic, and mechanically flexible. A detailed comparison of key capabilities and figures-of-merits with existing IR camouflage systems can be found in Table S3. Using a wet etch-transfer method (see Methods and Figure S5), the graded-WVO_2 film is transferred from the growth substrate onto a polyethylene (PE) tape. As the total thickness of the WVO_2 film is less than 100 nm, the WVO_2/tape structure can be bent to curvatures exceeding 10/cm (Figure 2c) without degrading its camouflage performance. The mechanical flexibility combined with the angular-independence of emissivity (Figure S6) allows the camouflage to be easily applied as a tape onto non-flat surfaces, with minimal or no impact to the performance (Figure S7). No noticeable degradation in camouflage property or change in surface morphology was detected after up to 100 heating/cooling cycles through the working temperature range (15-65 °C), demonstrating good reliability of the film (Figure S8). In Figure S8, A T_{IR} difference of ~ 3 °C is observed between the heating and cooling branches, caused by the hysteresis effect of the WVO_2 phase transition. This degree of impact should not affect the general applicability of the technique, and could be reduced by future work to optimize the hysteresis, including process by crystal dehydration[31] or Ti doping method[32].

A series of experiments were conducted to test the performance of the camouflage. Figure 2c shows optical image and IR snapshot of a finger where the tip is covered by the camouflage. Distinct from the exposed skin, the part covered by the camouflage displays a T_{IR} similar to the environment, concealing the fingertip from IR detection. Apart from such conventional application as a living body camouflage, our structure has the inherent, unique advantage to cover up objects with large spatial variation (∇T) or abrupt temporal fluctuation (dT/dt) of temperature. In Figure 2d, a copper plate coated with high-emissivity tape is thermally biased with T_{actual} varying from 25 °C to 65 °C. Three identical WVO_2 camouflages were placed at different positions of the plate that have distinct local temperatures. The regions underneath the camouflages are simultaneously masked from IR detection regardless of the different local temperatures and high thermal gradient. Compared to using multiplexing to address the spatial temperature variation in conventional camouflages[26, 29], the graded WVO_2 design offers a much simpler, monolithic, power-free and tetherless approach.

The camouflage is also inherently immune against abrupt temperature fluctuation. In Figure 2e, a heater membrane is partly covered by our graded WVO_2 film transferred onto a high-emissivity PE tape (sample), and the rest is covered by the high-emissivity PE tape alone (control). The temperature of the plate shoots up rapidly when a current pulse passes through the heater. The IR camera catches clearly a temperature spiking up to 65 °C within less than 2 seconds from the control surface, while the camouflaged surface stays at nearly constant T_{IR} of 20 °C irrespective of the heat pulse (see video in Supplementary Information, Video S1). The detected T_{IR} is plotted as a function of time in Figure 2f, which shows a nearly total immunity to the temperature surge. This immunity is a substantial advantage over the strategy of adjusting the emissivity using a feedback loop in conventional camouflages, as the latter typically has a response time over seconds[26, 27, 30] and would have the object exposed to detection during the response lagging time.

Next, we demonstrate another unique function, a thermal IR "decoy", using the structure. A decoy is different from the camouflage in the way that the decoy would not only passively conceal from IR camera the real thermal activity of the object, but also intentionally fool the camera with a counterfeited T_{IR} image that is independent of T_{actual} distribution and fluctuation. That is, to create a robust thermal radiative pattern $T_{IR}(X, Y, Z)$ on a surface that has arbitrary actual temperature distribution $T_{actual}(X, Y, Z, t)$, where X, Y and Z are the coordinates of the surface and t is time. Because the overall emissivity of the graded-WVO_2/tape system is the combined effect of both the WVO_2 film and the tape, by using different doping profiles for the graded WVO_2 film and transferring onto different tapes, T_{IR} of the camouflage can be designed to take distinct values to meet different requirements. A series of flexible WVO_2 / tape samples were prepared (details in Figure S9). As shown in Figure 3a, despite T_{actual} varying widely from room temperature to ~ 70°C, these samples all exhibit a nearly constant T_{IR} within the T_{actual} range, whereas T_{IR} is designed to be equal to any desired value in the range of 5 °C ~ 30 °C. As a proof of concept, Figure 3b and Figure 3c demonstrate a working decoy where the image of "CAL" shows a stable IR temperature reading, regardless of the change in T_{actual}. Such decoying information can be also encoded during the film deposition by laterally patterning the composition and thickness of the graded WVO_2 film, allowing fabrication of a monolithic and lithographically manufacturable decoy (Figure S10).

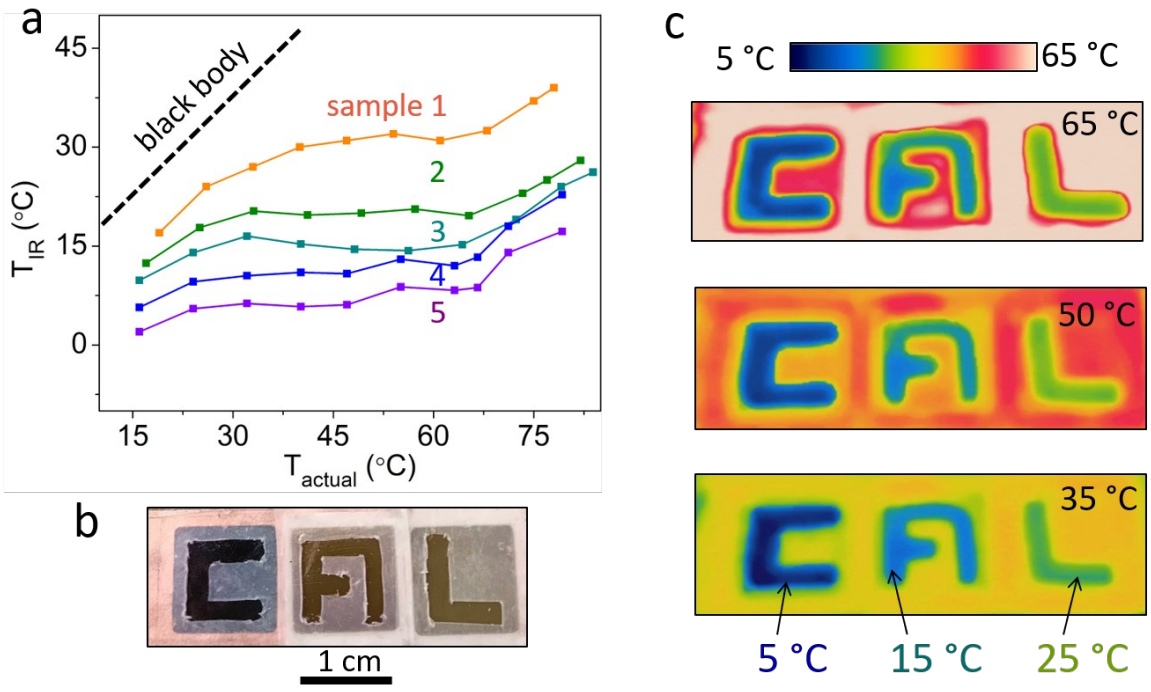

Figure 3. Demonstration of T_{actual}-independent thermal IR decoy. a*. IR temperature (T_{IR}) versus actual temperature (T_{actual}) of five flexible structures, where the graded WVO_2 configuration is designed to yield T_{actual}-independent, but different values of, desired T_{IR} within the working range of T_{actual}. Details of these samples are shown in Fig.S9. The error bars are comparable to the symbols in size.* ***b*** *(optical) and* ***c*** *(IR images), using the sample 1, 3 and 5, respectively, a pattern of "CAL" is made to show "C" at constant $T_{IR} \approx 5\ ^oC$, "A" at $T_{IR} \approx 15\ ^oC$ and "L" at $T_{IR} \approx 25^oC$, regardless of T_{actual} varying to 65, 50 or 35 ^oC. The three samples are all $1\times1\ cm^2$ in size.*

While these features greatly expand the application of radiative camouflage to inhomogeneous and dynamic environments as well as IR decoying, they also inspire novel device concepts based on reflection or transmission of IR signals. As expected, over the broad spectral range from near-IR (down to the plasma wavelength ~ 1.2 μm) to the far-IR, the reflectivity of the graded WVO_2 would exhibit a temperature dependence that is much

stronger than that of conventional materials (Figure S11 shows part of the spectrum). This feature enables potential ways for high-sensitivity remote temperature sensing using thermoreflectance imaging, or active reflectance modulation of IR signals. Therefore, the graded WVO_2 structure offers a general platform for unprecedented manipulation and processing of IR signals for novel radiative and reflective systems.

Experimental Section

Thin film deposition and etching/transfer process. WVO_2 thin films were grown on c-cut sapphire and quartz substrates using pulsed laser deposition (PLD). The graded W doping was achieved by sequentially focusing the pulsed laser on a series of WVO_2 targets with different W doping ratios. The targets were prepared by mixing WO_3 and V_2O_5 powders with W:V atomic ratio ranging from 0 to 3.0%, then made into 1 inch diameter round discs with a hydraulic press. All thin films were deposited in 5 mTorr O_2 environment at 475 °C substrate temperature. The PLD laser energy was set at 321 mJ with 5 Hz pulse frequency. A post-deposition anneal at 475 °C for 30 mins in the same 5mTorr O_2 environment was performed for all graded doped WVO_2 film. The thickness and deposition rate of the thin films were measured by atomic force microscopy and scanning electron microscopy (Figure S12), and the W faction as well as depth profile were characterized by x-ray photoelectron spectroscopy (Figure S3).

WVO_2 thin films grown on quartz substrates were transferred onto PE tapes by sticking the WVO_2 side to the adhesive side of the tape, and then etching off the 170 μm thick quartz substrate by dipping into 49% Hydrofluoric (HF) acid for 5 mins. The samples with transferred WVO_2 were then rinsed in deionized water for 3 mins and gently blown dry with a N_2 gun. The interfacial adhesion is strong and no delamination of WVO_2 is observed during the wet transfer process, in further contact with water, or with mechanical bending and twisting of the tape. The thickness of the PE tape (default) and the scotch tape is ~ 0.20 mm and 0.08 mm, respectively. The visible color of mainly depends on the thickness of the graded WVO_2 coating layer. Thicker film will appear blue/purple, while thinner film tends to have brown/yellow color. When taking a photo, the lighting and the reflection will affect the visible appearance of the sample surface as well.

FTIR measurements and IR imaging

The normal-direction emissivity $\varepsilon(\lambda,T)$ was obtained from normal-incident reflection measurements following the equation: $\varepsilon(\lambda,T) = 1 - R(\lambda,T)$, due to negligible transmission $T(\lambda,T)$ of the sample over the spectra of interest. The reflection spectra, $R(\lambda,T)$, were characterized by an Agilent Cary 670 FTIR spectrometer and Agilent Cary 620 microscope system with a 15× objective lens (numerical aperture of 0.62). A blade aperture of 60 μm × 60 μm was used to select the area of interest. For measurements of samples on PE tapes, flat regions away from substrate curving spots were chosen to minimize scattering, and multiple (> 3) measurements were performed to confirm repeatability of the results. All reflection spectra were normalized to the reflection spectrum of a 300 nm thick gold film. The temperature of the samples was controlled by a customized closed-loop thermal stage, connected to a Lakeshore 321 temperature controller.

The IR images and videos were captured by a FLIR ONE infrared camera. To avoid reflection signals from the camera and the surrounding, the default viewing angle was set as 15° instead of normal incident direction, and the experiments were performed in an open-area outdoor environment under clear sky (little cloud). The temperature was controlled by the same thermal stage used in the FTIR measurements. When taking an IR image, the camera measures the incident thermal radiation P_{rad}, and gives the temperature reading (T_{IR}) assuming a constant emissivity for the target ($\varepsilon_0 = 0.90$). The relationship can be described by the equation: $\varepsilon_0 \sigma T_{IR}^4 = P_{rad}$. The T_{IR} was then plotted as a function of actual temperature (T_{actual}) to demonstrate the camouflage performance.

The error bars for data presented in this work are based on standard deviation of at least 3 separate samples. This applies to both the figures in the manuscript and the supporting information.

Conflict of interest

The authors declare no conflict of interest

Supporting Information

Supporting Information is available from the Wiley Online Library or from the author.

Acknowledgements

This work was supported by the U.S. NSF Grant No. DMR-1608899. The materials preparation part was done at the Electronic Materials Program at the Lawrence Berkeley National Laboratory supported by Director, Office of Science, Office of Basic Energy Sciences, Materials Sciences and Engineering Division, of the U.S. Department of Energy under Contract No. DE-AC02-05CH11231. K. T. acknowledges the Bakar Spark Funds. X. W. and J. Y. acknowledge support from the U.S. National Science Foundation under grant No.1555336. C.W.Q. acknowledges support from the A*STAR Pharos Program (Grant No. 1527000014, with Project No. R-263- 000-B91-305). We thank Prof. Peter Fan Yang for helpful discussion.

Author Contributions

J.W. conceived the project. J.W. and K.T. designed the experiments. K.T. prepared the materials, fabricated the devices and performed the measurements. X. W. helped with training and measurements of the FTIR. X. Z. provided instrumental support for the FTIR

experiments. K. D. performed theoretical modeling. J. L. helped with preparation of the figures and SEM measurement. All authors contributed to discussing the data and editing the manuscript.

References

[1] F. J. Morin, *Phys. Rev. Lett.* **1959**, *3*, 34.

[2] J. Jian, X. Wang, L. Li, M. Fan, W. Zhang, J. Huang, Z. Qi, H. Wang, *ACS Applied Materials & Interfaces* **2017**, *9*, 5319.

[3] F. Ligmajer, L. Kejík, U. Tiwari, M. Qiu, J. Nag, M. Konečný, T. Šikola, W. Jin, R. F. Haglund, K. Appavoo, D. Y. Lei, *ACS Photonics* **2018**, *5*, 2561.

[4] M. M. Qazilbash, M. Brehm, B.-G. Chae, P.-C. Ho, G. O. Andreev, B.-J. Kim, S. J. Yun, A. V. Balatsky, M. B. Maple, F. Keilmann, H.-T. Kim, D. N. Basov, *Science* **2007**, *318*, 1750.

[5] V. Eyert, *Phys. Rev. Lett.* **2011**, *107*, 016401.

[6] A. S. Barker, H. W. Verleur, H. J. Guggenheim, *Phys. Rev. Lett.* **1966**, *17*, 1286.

[7] T. Ben-Messaoud, G. Landry, J. P. Gariépy, B. Ramamoorthy, P. V. Ashrit, A. Haché, *Opt. Commun.* **2008**, *281*, 6024.

[8] M. A. Kats, R. Blanchard, S. Zhang, P. Genevet, C. Ko, S. Ramanathan, F. Capasso, *Phys. Rev. X* **2013**, *3*, 041004.

[9] S. Wang, G. Liu, P. Hu, Y. Zhou, Y. Ke, C. Li, J. Chen, T. Cao, Y. Long, *Advanced Materials Interfaces* **2018**, *5*, 1801063.

[10] J. Agassi, *Science* **1967**, *156*, 30.

[11] K. Ito, K. Nishikawa, H. Iizuka, H. Toshiyoshi, *Appl. Phys. Lett.* **2014**, *105*, 253503.

[12] R. W. Boyd, *Radiometry and the Detection of Optical Radiation*, Wiley, New York 1983.

[13] D. Liu, H. Cheng, X. Xing, C. Zhang, W. Zheng, *nfrared Phys. Technol.* **2016**, *77*, 339.

[14] Z. Mao, W. Wang, Y. Liu, L. Zhang, H. Xu, Y. Zhong, *Thin Solid Films* **2014**, *558*, 208.

[15] S. Lee, K. Hippalgaonkar, F. Yang, J. Hong, C. Ko, J. Suh, K. Liu, K. Wang, J. J. Urban, X. Zhang, C. Dames, S. A. Hartnoll, O. Delaire, J. Wu, *Science* **2017**, *355*, 371.

[16] R. J. Thorn, O. C. Simpson, *J. Appl. Phys.* **1953**, *24*, 633.

[17] T. Satō, *Jpn. J. Appl. Phys.* **1967**, *6*, 339.

[18] A. H. Sully, E. A. Brandes, R. B. Waterhouse, *Br. J. Appl. Phys.* **1952**, *3*, 97.

[19] M. F. Modest, *Radiative Heat Transfer*, Elsevier Science, San Diego 2013.

[20] E. H. Putley, *Phys. Technol.* **1973**, *4*, 202.

[21] C. D. Tran, *Anal. Lett.* **2005**, *38*, 735.

[22] X. Liu, W. J. Padilla, *Adv. Mater.* **2016**, *28*, 871.

[23] L. Xiao, H. Ma, J. Liu, W. Zhao, Y. Jia, Q. Zhao, K. Liu, Y. Wu, Y. Wei, S. Fan, K. Jiang, *Nano Lett.* **2015**, *15*, 8365.

[24] H. Ji, D. Liu, H. Cheng, C. Zhang, L. Yang, D. Ren, *RSC Adv.* **2017**, *7*, 5189.

[25] P. Chandrasekhar, B. J. Zay, G. C. Birur, S. Rawal, E. A. Pierson, L. Kauder, T. Swanson, *Adv. Funct. Mater.* **2002**, *12*, 95.

[26] O. Salihoglu, H. B. Uzlu, O. Yakar, S. Aas, O. Balci, N. Kakenov, S. Balci, S. Olcum, S. Süzer, C. Kocabas, *Nano Lett.* **2018**, *18*, 4541.

[27] B. Kim, J. K. Koh, J. Park, C. Ahn, J. Ahn, J. H. Kim, S. Jeon, *Nano Convergence* **2015**, *2*, 19.

[28] J. Park, J.-H. Kang, X. Liu, S. J. Maddox, K. Tang, P. C. McIntyre, S. R. Bank, M. L. Brongersma, *Science Advances* **2018**, *4*, eaat3163.

[29] Z. J. Coppens, J. G. Valentine, *Adv. Mater.* **2017**, *29*, 1701275.

[30] C. Xu, G. T. Stiubianu, A. A. Gorodetsky, *Science* **2018**, *359*, 1495.

[31] X. Li, L. Yang, S. Zhang, X. Li, J. Chen, C. Huang, *Mater. Lett.* **2018**, *211*, 308.

[32] S. Chen, J. Liu, L. Wang, H. Luo, Y. Gao, *J. Phys. Chem. C* **2014**, *118*, 18938.